JOURNAL OF AIRCRAFT
Vol. 39, No. 6, November–December 2002

Automated Cruise Flap for Airfoil Drag Reduction over a Large Lift Range

Christopher W. McAvoy* and Ashok Gopalarathnam†
North Carolina State University, Raleigh, North Carolina 27695-7910

A small trailing-edge flap, often referred to as a cruise flap or camber-changing flap, can be used to extend the low-drag range of a natural-laminar-flow airfoil. Automation of such a cruise flap is likely to result in improved aircraft performance over a large speed range without an increase in the pilot work load. An important step in achieving the automation is to arrive at a simple approach for determination of the optimum flap angle for a given airfoil lift coefficient. This optimum flap angle can then be used in a closed-loop control system to set the flap automatically. Two pressure-based schemes are presented for determining the optimum flap angle for any given airfoil lift coefficient. The schemes use the pressure difference between two pressure sensors on the airfoil surface close to the leading edge. In each of the schemes, for a given lift coefficient, this nondimensionalized pressure difference is brought to a predetermined target value by deflecting the flap. It is shown that the drag bucket is then shifted to bracket the given lift coefficient. This nondimensional pressure difference, therefore, can be used to determine and set the optimum flap angle for a specified lift coefficient. The two schemes differ in the method used for the nondimensionalization. The effectiveness of the two schemes is verified using computational and wind-tunnel results for two NASA laminar flow airfoils. Finally, an aircraft performance simulation approach is used to analyze the potential aircraft performance benefits while addressing trim drag considerations.

Nomenclature

A_1	=	coefficient used in thin airfoil theory Fourier series
C_d	=	airfoil drag coefficient based on the chord
C_l	=	airfoil lift coefficient based on the chord
$C_{l\text{ideal}}$	=	airfoil C_l at which the stagnation point is located at the leading edge of the airfoil in thin airfoil theory
C_m	=	airfoil pitching-moment coefficient about the quarter-chord location
C_p	=	pressure coefficient
c	=	airfoil chord length
M	=	Mach number
p	=	pressure
q	=	dynamic pressure
Re	=	Reynolds number
x, y	=	coordinates
x_f	=	x coordinate of flap hinge
α	=	angle of attack
ΔC_p	=	difference in leading-edge pressures nondimensionalized by dynamic pressure
$\Delta C'_p$	=	difference in leading-edge pressures nondimensionalized by the absolute value of $(p_u - p_l)$
δ_f	=	flap deflection, rad
θ_f	=	angular coordinate of flap hinge, rad

Subscripts

l	=	location near midchord on the lower surface
ll	=	location near leading edge on the lower surface
lu	=	location near leading edge on the upper surface
u	=	location near midchord on the upper surface
0	=	stagnation-point condition
∞	=	refers to freestream condition

Received 27 November 2001; revision received 21 May 2002; accepted for publication 3 June 2002.

*Graduate Research Assistant, Department of Mechanical and Aerospace Engineering, Box 7910; cwmcavoy@eos.ncsu.edu. Student Member AIAA.
†Assistant Professor, Department of Mechanical and Aerospace Engineering, Box 7910; ashok_g@ncsu.edu. Member AIAA.

Introduction

IT is well known that the deflection of a small trailing-edge flap, often referred to as a "cruise flap," shifts the low-drag region of the airfoil drag polar. Positive, or downward, deflection of the trailing-edge flap causes the laminar drag bucket to shift to higher lift coefficients, whereas negative flap deflections cause a shift to lower lift coefficients. The desired shift in the drag bucket is accomplished when, for a given lift coefficient, the flap is deflected to the appropriate angle at which the leading-edge stagnation point is brought to the optimal position resulting in favorable pressure gradients on both the upper and lower surfaces of the airfoil.[1–4] Consequently, extended laminar flow and low airfoil profile drag are achieved over a wide range of lift coefficients and, hence, a wide range of aircraft speeds.

Originally conceived by Pfenninger[1,2] (also see Ref. 5) around 1947, cruise flaps have been used to good advantage in the design of many natural-laminar-flow (NLF) airfoils,[3,4,6–10] and these flaps have been widely used on high-performance sailplanes for several years. Cruise flaps also enable the use of airfoils with extended amounts of laminar flow. When the extents of the laminar flow are increased, the decrease in airfoil drag is accompanied by a reduction in the width of the drag bucket.[11,12] When cruise flaps are used, the drag bucket is effectively widened, and the high performance of the airplane is not restricted to a small range of flight speeds. In spite of these advantages, cruise flaps have not gained popularity for routine use on general aviation and other commercial aircraft. An important reason is believed to be the increase in pilot workload that accompanies the traditional installation of cruise flaps. Current use of cruise flaps requires the pilot to continuously monitor the airspeed and to adjust the flap to the optimum location using some form of a look-up table. Another problem with the current cruise flaps is that, unless they are to be extensive, the look-up tables connecting airspeed and flap angle are valid for only one flight condition, that is, one airplane weight, load factor, and center-of-gravity (c.g.) position. An automation of the cruise flap with a closed-loop control system would provide the benefits without any increase in the pilot workload. In addition, such an automated system would enable the use of cruise flaps on autonomous and uninhabited aerial vehicles (UAVs), where low drag is desirable over a wide range of flight conditions from loiter to dash.

A key ingredient in an automated cruise flap system is a scheme to determine the optimum flap deflection for any given lift coefficient. It would be desirable to have the scheme be independent of changes in weight, load factor, and c.g. position. For this reason, it is preferable to avoid a system that sets the flap angle based on the aircraft lift coefficient computed from the measured airspeed. The objective of the current work has been to develop a simple approach for determining the optimum flap deflection angle for a given airfoil lift coefficient. In this paper, a concept is presented in which the difference between two pressure measurements on the airfoil surface is nondimensionalized and used to determine the best flap deflection angle. The concept is presented and demonstrated first using computational and experimental results for the NASA NLF(1)-0215F airfoil, along with two possible schemes for the implementation. The schemes are then also shown to be valid for another flapped airfoil, the NASA NLF(1)-0414F, again using both computational and experimental results. These two particular NASA airfoils have been chosen because they have both been designed and wind-tunnel tested with cruise flaps, and extensive surface pressure data are available in the NASA reports.[3,6] Finally, a section is presented on the integration of automated cruise flaps on aircraft, including an analysis of potential aircraft performance benefits using a hypothetical long-range UAV with a customized flapped NLF airfoil as an example.

Flow Sensing Approaches for Flap Automation

In this section, two flow sensing approaches for flap automation are presented using the flapped NASA NLF(1)-0215F airfoil as an example. The first approach involves sensing of the stagnation point, and the second approach involves the use of pressure sensing at the leading edge. The NLF(1)-0215F airfoil has been analyzed using XFOIL[13] at several flap angles. In these and all of the other XFOIL analyses in this paper, free transition was assumed. With this assumption, the transition locations were computed as a part of the solution using an approximate e^n-type transition amplification formulation. A value of $n_{crit} = 9$ was assumed for the critical amplification factor in all of the XFOIL results in this paper. The drag polars and pressure distributions from XFOIL are examined to first study the variation of the leading-edge stagnation-point location with airfoil lift coefficient and flap angle. Two pressure-based schemes are then proposed for determining the best flap angle for a given lift coefficient. In each scheme, the nondimensional difference between the static pressures measured at two locations on the airfoil surface is required to be held at a constant value by adjusting the flap angle. The two schemes differ in the pressure value used for the nondimensionalization. The pressure-based schemes are demonstrated using the XFOIL computational results, as well as using the detailed experimental data from the NASA wind-tunnel tests for the NLF(1)-0215F airfoil.[6]

Figure 1 shows the geometry of the NASA NLF(1)-0215F airfoil along with the pressure distributions from XFOIL analyses at lift coefficients when operating within the drag bucket, at flap deflections of −10, −5, 0, 5, and 10 deg. A 0.25c flap has been used for these computations with the hinge located at $x/c = 0.75$ and $y/c = 0.0328$ to correspond with the hinge location used in the wind-tunnel investigation reported in Ref. 6. Figures 2a and 2b show the predicted performance for this airfoil from XFOIL analyses and from the NASA wind-tunnel results, respectively, for a Reynolds number of 6×10^6. First, it is seen that although the XFOIL predictions and the wind-tunnel results do not agree perfectly with each other, the trends compare very well. Next, it is readily seen that deflection of the flap from −10 to 10 deg results in low drag over a wide C_l range from 0.2 to 1.31. On the other hand, if zero flap deflection is used, the low airfoil drag is restricted to a smaller C_l range from 0.56 to 0.98. This benefit is the reason for integration of cruise flaps in the design of many NLF airfoils including the NASA NLF(1)-0215F,[6] NASA NLF(1)-0414F,[3,4] Althaus and Wortmann,[8] and Drela[9] sailplane airfoils. More recently, aerodynamic methods have also been developed for inverse design of airfoils with cruise flaps.[14]

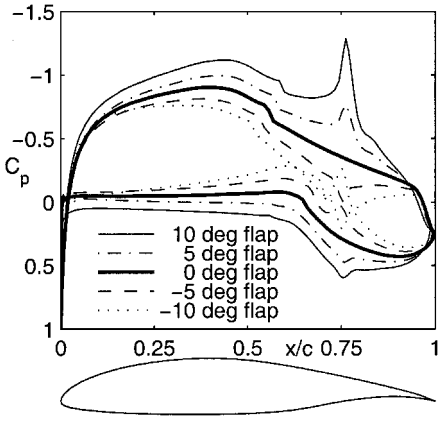

Fig. 1 NLF(1)-0215F airfoil geometry and pressure distributions from XFOIL analyses at $Re = 6 \times 10^6$ for different flap deflections with the airfoil operating within the drag bucket.

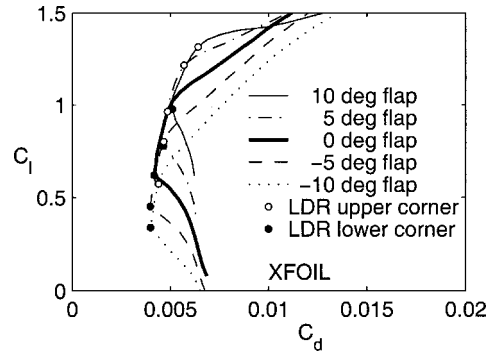

a) From XFOIL analyses

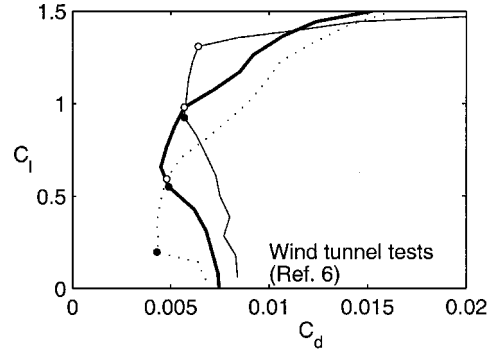

b) From wind-tunnel experiments.[6]

Fig. 2 Predicted and experimental results for the drag polars of the flapped NLF(1)-0215F airfoil at a Reynolds number of 6×10^6 along with the upper and lower corners of the LDR for each case.

Stagnation-Point Location Sensing

To understand how a cruise flap extends the low-drag range (LDR) of the airfoil drag polar, the role of the leading-edge stagnation point is first examined. The variation of the leading-edge stagnation point with C_l for different flap settings is shown for the NLF(1)-0215F airfoil in Fig. 3 along with the points corresponding to the corners of the LDR for each flap deflection. Figure 3 shows that, irrespective of the flap setting, there is a small desirable region for the leading-edge stagnation point, shown in Fig. 4, that always results in low airfoil drag by promoting laminar flow on both surfaces of the airfoil.

Note that this observation can be deduced even from thin airfoil theory. From thin airfoil theory, it is possible to compute the $C_{l\,\text{ideal}}$ corresponding to the ideal angle of attack[15,16] at which the stagnation point is exactly at the leading edge of the thin airfoil. At this condition, there are no singularities (or suction peaks) on either the upper or the lower surface. This condition corresponds closely to the C_l for the middle of the LDR. The expression for $C_{l\,\text{ideal}}$ for a thin

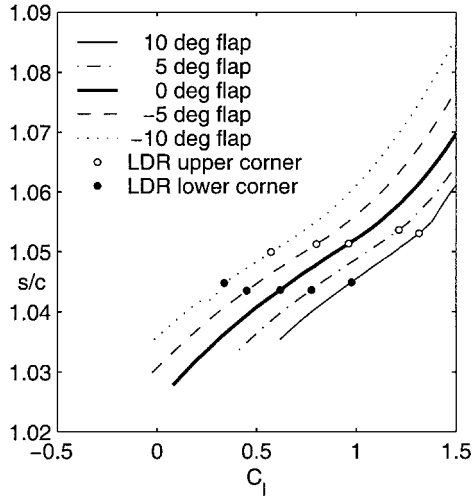

Fig. 3 Variation of the stagnation-point location with airfoil lift coefficient for flap deflections of −10, −5, 0, 5, and 10 deg.

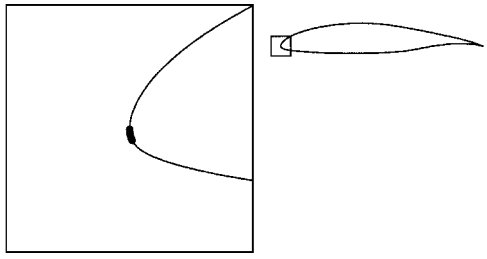

Fig. 4 Geometry of the airfoil with inset showing desired range for stagnation-point location.

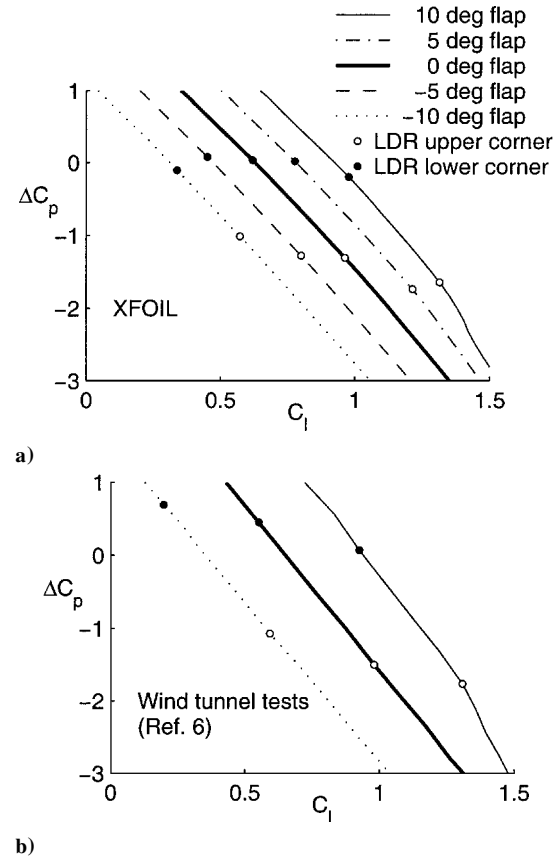

Fig. 5 Predicted and experimental results for the ΔC_p for the NLF(1)-0215F airfoil from a) XFOIL analyses and b) wind-tunnel experiments.[6]

symmetric airfoil with a trailing-edge flap hinged at x_f/c is shown in Eq. (1), where A_1 is one of the coefficients in the Fourier series traditionally used to represent the chordwise vorticity distribution in thin airfoil theory (see Ref. 17). The angular coordinate for the hinge location θ_f is related to x_f/c as shown in Eq. (2). When a thin airfoil is analyzed with a 25%-chord trailing-edge flap, it can be seen from Eq. (1) that the $C_{l\,\text{ideal}}$ increases by 0.3 for every 10 deg of positive flap deflection. This result is close to the predicted shift in the LDR seen from the XFOIL analyses and the experimental results in Fig. 2.

$$C_{l\,\text{ideal}} = \pi A_1 = 2\delta_f \sin\theta_f \tag{1}$$

$$\theta_f = \cos^{-1}[1 - 2(x_f/c)] \tag{2}$$

Thus, if the stagnation point could be detected in real time, a system could be created that deflects the cruise flap to maintain the stagnation point in the optimum region. Whereas it is possible to detect the location of the stagnation point using surface hot-film arrays,[18,19] the current paper focuses on use of simpler surface pressure measurements for indirectly detecting the effects of the stagnation-point location.

Surface Pressure Sensing

To illustrate the key idea behind the simpler pressure-based method for determining the optimum flap deflection, the pressure distributions shown in Fig. 1 for the NLF(1)-0215F airfoil when operating within the drag bucket with different flap deflections are examined. From Fig. 1, it is seen that, independent of the flap angle, the pressure distributions in the vicinity of the leading edge are very similar when the airfoil is operating in the LDR. This result is not surprising considering that the stagnation-point location is nearly independent of the flap angle, as seen from Figs. 3 and 4, when the airfoil is operating within the LDR. When the plots in Fig. 1 were examined it was hypothesized that the difference in pressure coefficients measured from two pressure sensors close to the leading edge could provide a measure of whether the airfoil is operating within the drag bucket, irrespective of the flap angle.

To verify this hypothesis, the XFOIL and wind-tunnel results for the NLF airfoil were used to determine the pressure-coefficient difference ΔC_p between the 2%-chord location on the upper surface and the 2%-chord location on the lower surface. Figures 5a and 5b show how this ΔC_p varies with C_l for the different flap deflections from the XFOIL analyses and experimental results, respectively. It is clearly seen that, irrespective of the flap angle, there is a region of values of ΔC_p that, when achieved, ensures operation of the airfoil in the low drag region of the polar. Additional analysis of this relationship has shown that, although the method is not highly sensitive to the exact location of the pressure taps, it is desirable to measure the pressures closer to the airfoil leading edge to obtain a larger variation in ΔC_p for a given change in airfoil C_l. The reason for this larger variation is that the pressures closer to the leading edge are more sensitive to the movement of the stagnation point.

Although there is a possibility that the use of pressure orifices in the vicinity of the leading edge may cause premature transition, there is evidence that a small-diameter pressure orifice in a favorable pressure gradient is less likely to cause premature transition than one in an adverse pressure gradient.[20] Because the pressure orifices located in the vicinity of the leading edge will be in regions of favorable pressure gradient when the airfoil operates within the LDR, it is believed that these pressure orifices are unlikely to cause premature transition for the operating conditions of interest.

It must be remembered, however, that the difference in the measured surface pressure ($p_{lu} - p_{ll}$) needs to be nondimensionalized to determine the ΔC_p. As seen from Eq. (3), this nondimensionalization can be readily done by dividing the pressure difference by the dynamic pressure measured by the aircraft pitot–static system:

$$\Delta C_p = \frac{p_{lu} - p_{ll}}{q_\infty} = \frac{p_{lu} - p_{ll}}{p_0 - p_\infty} = C_{p\,lu} - C_{p\,ll} \tag{3}$$

Although this scheme for nondimensionalization is sufficient, it has some drawbacks: 1) It is dependent on a pitot–static pressure

measurement that may be physically located far from the airfoil, resulting in pressure lag errors. 2) The measured static pressure usually has position errors that vary with the aircraft flight condition and are often dependent on whether or not the flaps are deployed. 3) The dynamic pressure measured by a pitot–static system that is located far away from the airfoil may not accurately reflect that experienced by the airfoil if the airplane has significant angular velocity. Moreover, a scheme that can determine the optimum flap location without having to depend on an independent measurement of the dynamic pressure may have the advantage that different airfoil sections on the lifting surfaces of an aircraft may be able to control independently the respective flap angles using self-contained pressure-based sensing systems in each of the sections. For these reasons, it is desirable to arrive at an alternate scheme for automating the cruise-flap setting.

To avoid the drawbacks associated with the use of aircraft dynamic pressure for the nondimensionalization, several alternate schemes were investigated. An alternate scheme is presented that involves a substitute for the dynamic pressure used for the nondimensionalization in Eq. (3). This second scheme involves the use of the absolute value of the difference between pressure measurements made near the midchord locations on the upper and lower surfaces of the airfoil. In other words, an alternate nondimensionalization is used to define a $\Delta C'_p$, where the denominator is the absolute value of $(p_u - p_l)$, as shown in Eq. (4). The drawback with this second scheme is that the $\Delta C'_p$ tends toward infinity when p_u nearly equals p_l. This condition may occur on an aircraft wing when using negative flap angles and when the airfoil lift coefficient is negative or close to zero. For most normal flight conditions and typical airfoils, this drawback is not a source for concern. Thus,

$$\Delta C'_p = \frac{p_{lu} - p_{ll}}{|p_u - p_l|} = \frac{C_{p_{lu}} - C_{p_{ll}}}{|C_{p_u} - C_{p_l}|} \tag{4}$$

In this paper, the locations for the upper- and lower-surface pressure measurements p_u and p_l are chosen to be at the downstream ends of the design extents of laminar flow on the upper and lower surfaces for the airfoil under consideration. This choice of locations for p_u and p_l has been made to reduce the possibility of premature transition due to the pressure orifices and the resulting loss in laminar flow. For the NASA NLF(1)-0215F airfoil used in this section, these locations correspond to $0.4c$ on the upper surface and $0.6c$ on the lower surface.

Figures 6a and 6b show the variation in $\Delta C'_p$ with C_l for the NLF(1)-0215 airfoil for the different flap deflections. As seen from these Figs. 6a and 6b, although the curves are less linear than those seen in Figs. 5a and 5b, there is a distinct range of $\Delta C'_p$ values for which the airfoil always operates within the drag bucket regardless of the flap angle.

In the following section, these two schemes, that is, the first scheme in which dynamic pressure is used for the nondimensionalization and the second scheme in which $|p_u - p_l|$ is used for the nondimensionalization, are both further validated using both computations and wind-tunnel data for the NASA NLF(1)-0414 airfoil. Figure 7 shows the geometry of this airfoil and the inviscid C_p distribution at $C_l = 0.4$.

Verification of the Schemes for the NLF(1)-0414F Airfoil

The NLF(1)-0414F airfoil was tested in the wind tunnel[3] with a $0.125c$ trailing-edge flap. Measured lift, drag, and moment data along with pressure distributions from surface-pressure orifices are documented in Ref. 3 for flap angles of -10, -5, 0, 5, and 10 deg at a Reynolds number of 10×10^6. As was done in the preceding section, the two pressure-based schemes are verified using both computational analyses and the results from the NASA wind-tunnel tests.[3]

The predicted and experimental drag polars for this airfoil are shown in Figs. 8a and 8b. As seen, the NLF(1)-0414F has a considerably narrower LDR than the NLF(1)-0215F because of the larger extents of laminar flow as well as the higher Reynolds number. As a result of the smaller LDR, an automated cruise flap system will

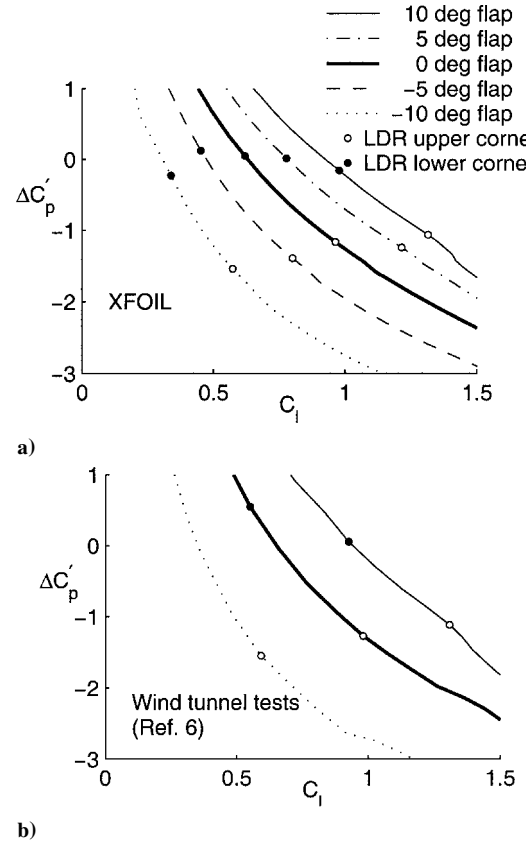

Fig. 6 Predicted and experimental results for the $\Delta C'_p$ for the NLF(1)-0215F airfoil from a) XFOIL analyses and b) wind-tunnel experiments.[6]

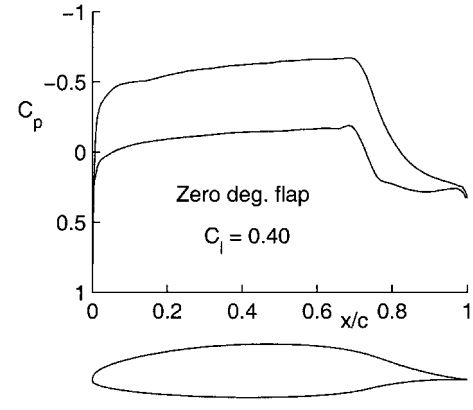

Fig. 7 NLF(1)-0414F airfoil geometry and inviscid C_p distribution.

be of significant benefit when used with this airfoil. For the same reason, this airfoil is a good test case for the two pressure-based schemes in this paper. Figures 9a and 9b show the effectiveness of the first scheme in plots of the ΔC_p from computational results and from the wind-tunnel data. The effectiveness of the second scheme is shown in Figs. 10a and 10b, where the $\Delta C'_p$ from computational results and wind-tunnel tests are plotted for the different flap angles. In both cases, for this airfoil, the leading-edge pressure differences $(p_{lu} - p_{ll})$ are the differences in pressure between the upper-surface $2\%c$ and the lower-surface $2\%c$ locations. For the $\Delta C'_p$, the p_u and p_l correspond to surface pressures at the $0.6c$ location on the upper surface and the $0.6c$ location on the lower surface, respectively. From Figs. 9 and 10, it is seen that both the computational results and the experimental data verify the effectiveness of the two pressure-based schemes for flap-angle automation.

Although the results from the XFOIL predictions and the NASA experiments do not agree perfectly with each other, it is clear that the trends compare well for both the NLF(1)-0215F and the

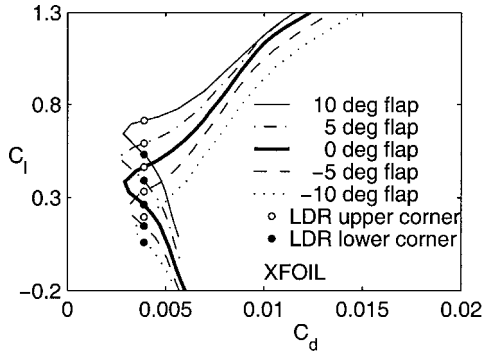

a) From XFOIL analyses

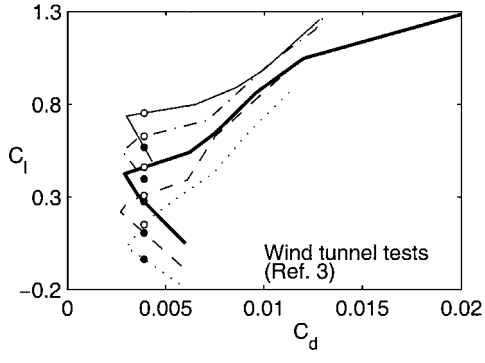

b) From wind-tunnel experiments.[3]

Fig. 8 Predicted and experimental results for the drag polars of the flapped NLF(1)-0414F airfoil at a Reynolds number of 10×10^6.

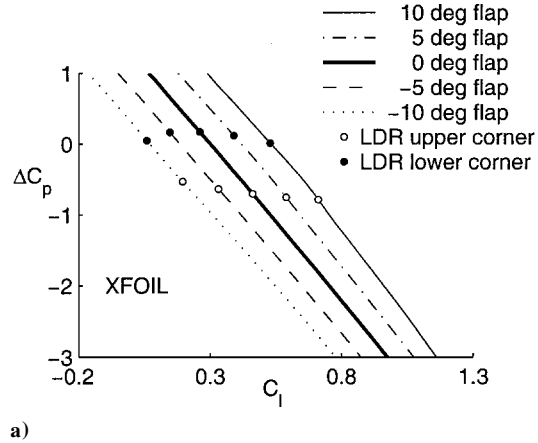

a)

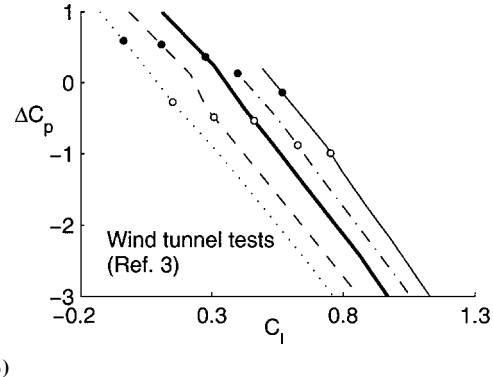

b)

Fig. 9 Predicted and experimental results for the ΔC_p for the NLF(1)-0414F airfoil from a) XFOIL and b) wind-tunnel experiments.[3]

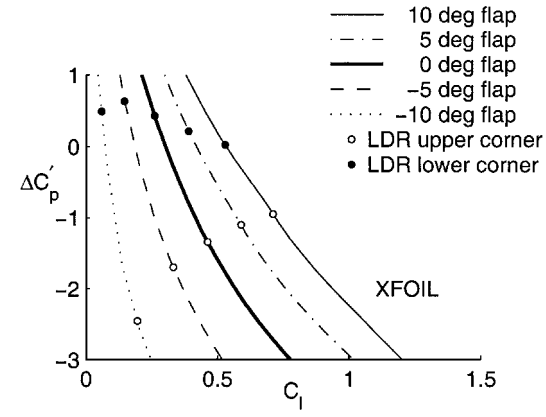

a)

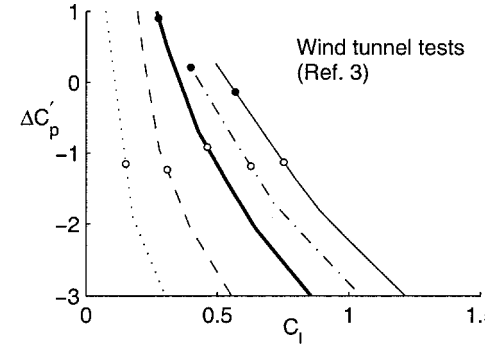

b)

Fig. 10 Predicted and experimental results for the $\Delta C_p'$ for the NLF(1)-0414F airfoil from a) XFOIL and b) wind-tunnel experiments.[3]

NLF(1)-0414F airfoils. More important, the computational and experimental results both demonstrate that either of the two schemes could be used to set the optimum flap angle for a given C_l by achieving a target value either for the ΔC_p or for the $\Delta C_p'$.

Implementation of the Schemes on Aircraft

The development of the simple pressure-based schemes described in this paper is believed to be an important step in the automation of cruise flaps for achieving improved performance over a large speed range for subsonic aircraft. Whereas the verification of the schemes have been presented for two-dimensional flow, the concept can be implemented on an aircraft wing. For application on an aircraft wing, a section of the wing should be chosen for which the section C_l is close to the wing C_L. On this wing section, the difference between the pressures measured at the two leading-edge pressure sensors can be nondimensionalized and used to drive the cruise flap to the correct angle. Algorithms for this closed-loop control do need to be developed and tested before the entire system can be implemented on an aircraft. Pending the development of the entire closed-loop system, the nondimensional leading-edge pressure difference, as described in this paper, can be used as such to drive a display in the cockpit that provides an easy means for the pilot to adjust the cruise flap to the correct angle.

Integration of cruise flaps on wings with control surfaces and high-lift flaps may require special consideration. For many aircraft concepts, it may be possible to design the flaps and control surfaces on the wing to double as cruise flaps. Also, cruise flaps could be integrated in the design of Fowler flaps by either incorporating a smaller-chord cruise flap at the trailing edge of a larger-chord Fowler flap as was done on the Cirrus VK30 experimental aircraft[21] or by allowing contour change of the Fowler flaps using modern form-variable structures.[22]

The pressure-based sensing approach described in this paper can also be used for stall warning, in a manner similar to that described in Ref. 23. The use for stall warning is possible because, for a given flap angle, the ΔC_p and $\Delta C_p'$ curves have one-to-one relationships

with the airfoil C_l up to the onset of stall. Thus, if the ΔC_p or $\Delta C'_p$ is known along with the flap angle, the section C_l can be determined. Additionally, the described schemes can be used with multiple, segmented trailing-edge flaps along the wing span, with the ΔC_p or $\Delta C'_p$ for each segment of the wing controlling the respective flap section. This concept allows for the tailoring of not only the local section profile drag but also the spanwise lift and C_l distributions. Thus, the concept paves the way for a section-C_l sensing method that can be used for in-flight minimization of the induced drag, tailoring of the spanwise stall behavior on the wing, and spanwise load redistribution during maneuvering conditions.

Interesting observations can also be made by comparing the airfoil drag polars, C_l, and C_m curves for an airfoil without cruise flaps and for one with an automated cruise-flap system. To illustrate these differences, a flapped NLF airfoil has been designed for application on a hypothetical UAV. The geometry and inviscid C_p distribution for this airfoil are shown in Fig. 11. The airfoil has been designed to support laminar flow to approximately $0.7c$ on both the upper and lower surfaces. A $0.15c$ cruise flap is used to extend the width of the LDR. To postpone the positive flap deflection at which the flow separates on the flap upper surface, the upper surface of the airfoil in the vicinity of the hinge has been specially contoured, resulting in a depression in the inviscid C_p distribution at $0.85c$ on the upper surface at the zero-flap condition. Such a flap-region contour tailoring is frequently done on flapped sailplane airfoils such as the FX 78-K-161/20 (Ref. 10).

To examine the behavior of this airfoil with an automated cruise flap, it is assumed that a target value of the $\Delta C'_p$ of -1 will be achieved by deflecting the flap to the required angle. Figure 12 shows

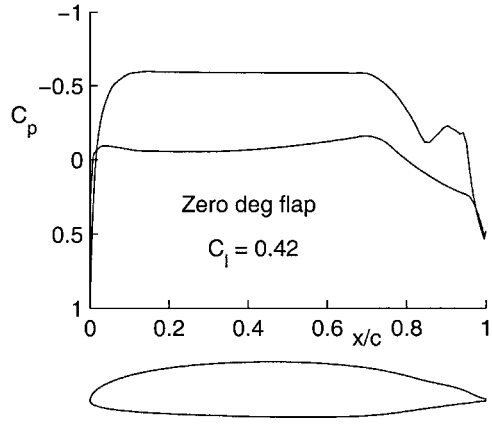

Fig. 11 Geometry and inviscid C_p distribution for the example NLF airfoil.

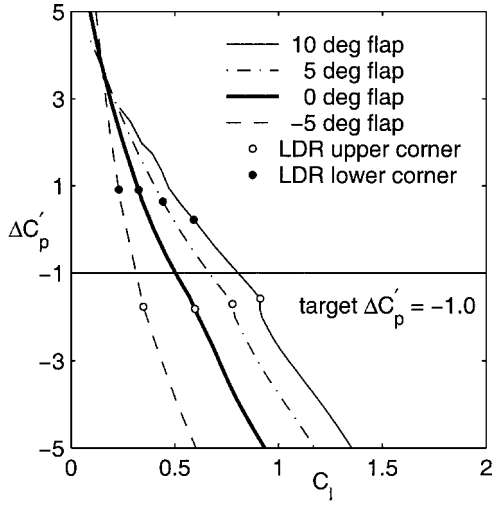

Fig. 12 Predicted results for the $\Delta C'_p$ for the example NLF airfoil from XFOIL analyses.

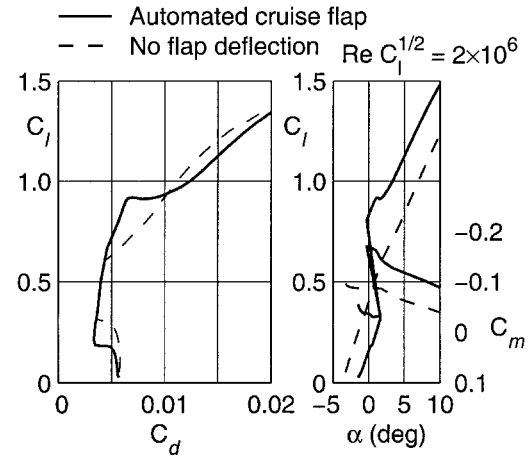

Fig. 13 Comparison of the drag polars and lift and pitching-moment curves for the example NLF airfoil with automated cruise flaps and without flaps.

the variation of $\Delta C'_p$ obtained from XFOIL analyses plotted against C_l for different flap deflections, with the upper and lower corners of the LDR marked for each case. Also shown is the target value of -1, which, if maintained, will result in the airfoil operating within the LDR for the range of flap deflections considered. The minimum and maximum angles for the cruise flap have been set to -5 and $+10$ deg, respectively. At flap angles much larger than $+10$ deg, the flow separates on the upper surface of the flap, resulting in an increase in the drag. Flap angles less than -5 deg do not provide benefits for the application considered.

The resulting drag polar for the airfoil with the automated cruise-flap system is compared in Fig. 13 to the drag polar of the airfoil without a cruise flap. Unlike the results for the NASA NLF airfoils shown earlier, the polars for this airfoil have been plotted at a constant value of reduced Reynolds number, $Re\sqrt{C_l} = 2 \times 10^6$. The use of a constant reduced Reynolds number ensures that the changes in Reynolds number with C_l due to changes in the flight velocity are automatically taken into consideration. From Fig. 13, although the large increase in the C_l range for low drag is clear, it is seen that for the automated-flap case, the change in α required for an increase in C_l is a small negative value. This differs from the usual lift-curve slope of approximately 2π/rad for the airfoil without the cruise flap. Additionally, the airfoil C_m about the quarter chord has a large variation when an automated cruise flap is used instead of a nearly constant C_m for an airfoil without a cruise flap. The nearly constant α for a wide C_l range for the automated-flap case may prove quite beneficial because the fuselage and nacelles can be optimized for a small variation in the aircraft α. The unusual variations in the C_l and C_m for the automated-flap case, however, do need to be analyzed in the context of how they may affect trim drag and, thus, overall aircraft performance. In particular, it is not clear if the large changes in C_m and any resulting trim drag will outweigh the profile drag reduction due to the cruise flaps. To address this issue, the characteristics of the NLF airfoil with and without the cruise flap have been used as inputs to the aircraft performance-simulation method described in Ref. 24 for a hypothetical UAV.

The hypothetical UAV for this illustration is assumed to have the characteristics listed in Table 1 and is assumed to have the wing–tail planform shown in Fig. 14. Because the primary purpose of the performance simulation is to compare the airfoil with and without a cruise flap, the propeller efficiency and specific fuel consumption for the powerplant have been assumed as constants for simplicity. The method, however, can readily accommodate nonconstant values for these parameters. As described in Ref. 24, the method first computes a drag buildup in which the total aircraft drag polar is obtained by summing the airfoil C_d shown in Fig. 13, a calculated aircraft C_{D_i}, and an assumed constant fuselage parasite drag. The aircraft C_{D_i} variation was obtained from a trim analysis of the wing–tail combination shown in Fig. 14. This analysis was performed using

Table 1 Assumed geometry, drag, and power characteristics for the hypothetical UAV

Parameter	Value
Gross weight	10231 N (2300 lbf)
Reference area	10.5 m^2 (113 ft^2)
Wing aspect ratio	21.4
Equivalent parasite drag area of airplane minus wing	0.12 m^2 (1.29 ft^2)
Rated engine power	74.63 k*W* (100 hp)
Specific fuel consumption	10.7 N/s/W (0.5 lbf/h/hp)
Propeller efficiency	85%, constant
Fuel volume	380 liters (100 U.S. gallons)
Tail area	3.06 m^2 (32.94 ft^2)
Static margin	15% Mean aerodynamic chord

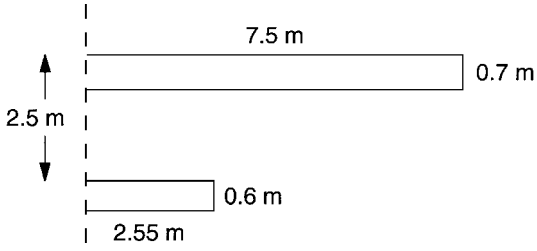

Fig. 14 Planview showing the right-side geometry of the wing and tail for the hypothetical UAV.

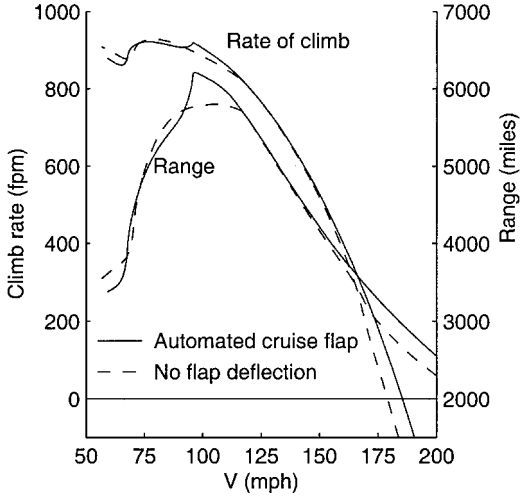

Fig. 15 Variation of UAV rate of climb and range with airspeed for the NLF airfoil with and without the automatic cruise flap.

Wings, a vortex-lattice code that can handle multiple lifting surfaces and has the capability to read XFOIL α, C_l, C_d, and C_m polar output files for the airfoils used for the lifting surfaces. In the current analysis, the horizontal tail incidence is adjusted to trim the aircraft, so that $C_{M_{cg}} = 0$. In other words, the drag contributions associated with the trim considerations have been included.

Figure 15 shows the variations of aircraft rate of climb and range with airspeed for the NLF airfoil both with zero flap deflection and with an automatic cruise flap. These performance parameters have been computed for sea-level conditions. The range computations have been performed using the well-known Bréguet range equation. In these range computations, the aircraft C_L has been assumed constant during the flight and the aircraft airspeed varied during the flight owing to decreasing fuel weight. The velocity used for the range curves in Fig. 15 corresponds to the gross-weight condition for the UAV. Comparison of the curves shows that despite the trim effects resulting from the unusual airfoil pitching-moment variations, the aircraft with the automated cruise flap performs considerably better over nearly the entire velocity range except for the region of zero flap deflection, where the performance is the same. The level-flight maximum speed at full throttle is the speed at which the rate of climb is zero. In this example, it is seen that the level-flight maximum speed is increased by approximately 6.5 mph as the result of using the automatic cruise flap. Also, the maximum range is increased by 425 miles and the range at the level-flight maximum speed is increased by nearly 300 miles. The maximum rate of climb remains approximately the same, but occurs at a higher velocity.

Although the aircraft performance benefits have been illustrated, the unusual variations in the C_l and C_m for the automated-flap case in Fig. 13 do need to be revisited in the context of how they may affect the aircraft static and dynamic stability and control characteristics. For example, because of the change in the airfoil C_m due to flap deflection and its effect on the aircraft trim, it may be necessary that the control of the cruise flap be coupled with the control of the elevator angle to maintain trimmed flight at a desired speed.

Conclusions

A trailing-edge cruise-flap system, when automated, has the potential to result in low airfoil drag over a wide C_l range. An important step toward the automation is a method to determine the correct flap angle that will result in extended laminar flow on both the upper and lower surfaces of the airfoil at a given C_l. To arrive at such a method, this paper draws on the well-known fact that a cruise flap results in a wide LDR by bringing the stagnation point to the small desirable region close to the leading edge. This small desirable region is quantified, and flow sensing approaches for detecting the stagnation point are then discussed. The paper then presents an approach where the nondimensional pressure difference between two points on the airfoil surface close to the leading edge can be used to set the cruise flap at the correct angle. It is shown that, independent of the flap angle, there is a band of values for this nondimensional pressure difference that, when achieved, will result in the airfoil operating within the LDR.

Two schemes have been presented for the nondimensionalization: the first in which the dynamic pressure is used and the second in which the pressure difference between the upper-surface and lower-surface locations near the midchord region of the airfoil is used for the nondimensionalization. The advantage of the first scheme is that only two pressure sensors are required, whereas the second scheme requires four pressure sensors. The first approach, however, has the disadvantage of being dependent on the dynamic pressure measured by the aircraft pitot–static system, whereas the second scheme results in a system that relies on measurements made entirely on the airfoil section under consideration. Computational and wind-tunnel results for two NASA laminar flow airfoils are used to verify the effectiveness of the two schemes.

Issues associated with the implementation of cruise flaps on aircraft are then discussed. To address the issue of whether the trim-drag increase due to changes in airfoil C_m with flap deflection outweighs the profile-drag benefits of cruise flaps, the effects on the performance of an example UAV have been presented. For the example used, the results clearly demonstrate the benefits of an automated cruise flap.

The results in the paper also show that the pressure-sensing schemes can be used to determine the operating C_l of an airfoil section inflight by knowing the value of the non-dimensional pressure difference. This capability results in the potential for further benefits such as stall warning and the use of segmented flaps along the span for tailoring the spanwise lift and C_l distributions that, in turn, allows for the control of induced drag, the tailoring of spanwise stall behavior, and the redistribution of the spanwise loads on a wing. This capability may, therefore, be useful for aerodynamic sensing on future adaptive aircraft concepts.

References

[1]Pfenninger, W., "Investigation on Reductions of Friction on Wings, in Particular by Means of Boundary Layer Suction," NACA TM 1181, Aug. 1947.

[2]Pfenninger, W., "Experiments on a Laminar Suction Airfoil of 17 Per Cent Thickness," *Journal of the Aeronautical Sciences*, Vol. 16, No. 4, 1949, pp. 227–236.

[3]McGhee, R. J., Viken, J. K., Pfenninger, W., Beasley, W. D., and Harvey, W. D., "Experimental Results for a Flapped Natural-Laminar-Flow Airfoil with High Lift/Drag Ratio," NASA TM 85788, May 1984.

[4]Viken, J. K., "Boundary-Layer Stability and Airfoil Design," *Laminar Flow Aircraft Certification*, NASA CP 2413, 1985, pp. 1–30.

[5]Wortmann, F. X., "Progress in the Design of Low Drag Airfoils," *Boundary Layer and Flow Control*, edited by G. V. Lachmann, Pergamon Press, New York, 1961, pp. 748–770.

[6]Somers, D. M., "Design and Experimental Results for a Flapped Natural-Laminar-Flow Airfoil for General Aviation Applications," NASA TP 1865, June 1981.

[7]Viken, J. K., "Aerodynamic Design Considerations and Theoretical Results for a High Reynolds Number Natural Laminar Airfoil," M.S. Thesis, George Washington Univ., Washington, DC, Feb. 1983.

[8]Althaus, D., and Wortmann, F. X., *Stuttgarter Profilkatalog I*, Friedr. Vieweg and Sohn Verlagsgesellschaft mbH, Vieweg, Braunschweig, Germany, 1981.

[9]Drela, M., "Elements of Airfoil Design Methodology," *Applied Computational Aerodynamics*, edited by P. A. Henne, Vol. 125, AIAA, Washington, DC, 1990, pp. 167–189.

[10]Althaus, D., *Niedrig-geschwindigkeits-profile*, Friedr. Vieweg and Sohn Verlagsgesellschaft mbH, Vieweg, Braunschweig, Germany, 1996.

[11]Wortmann, F. X., "A Critical Review of the Physical Aspects of Airfoil Design at Low Mach Numbers," *Motorless Flight Research*, edited by J. L. Nash-Weber, NASA CR 2315, Nov. 1973.

[12]Gopalarathnam, A., and Selig, M. S., "Low Speed Natural-Laminar-Flow Airfoils: Case Study in Inverse Airfoil Design," *Journal of Aircraft*, Vol. 38, No. 1, 2001, pp. 57–63.

[13]Drela, M., "XFOIL: An Analysis and Design System for Low Reynolds Number Airfoils," *Low Reynolds Number Aerodynamics*, edited by T. J. Mueller, Vol. 54, Lecture Notes in Engineering, Springer-Verlag, New York, 1989, pp. 1–12.

[14]Gopalarathnam, A., and Selig, M. S., "A Hybrid Approach to Inverse Design of Complex Aerodynamic Systems," AIAA Paper 2000-0784, Jan. 2000.

[15]Theodorsen, T., "On the Theory of Wing Sections with Particular Reference to the Lift Distribution," NASA TR 383, 1931.

[16]Abbott, I. H., and von Doenhoff, A. E., *Theory of Wing Sections*, Dover, New York, 1959, pp. 70–76.

[17]Katz, J., and Plotkin, A., *Low Speed Aerodynamics*, 2nd ed., Cambridge Univ. Press, New York, 2001, pp. 104–114.

[18]Mangalam, S. M., Wusk, M. S., and Kuppa, S., "In-Flight Detection of Stagnation, Transition and Separation Using Micro-Thin Surface Hot Films," *Proceedings of the 22nd Annual Symposium of the Society of Flight Tests Engineers*, 1991, pp. 1.2-1–1.2-12.

[19]Scott, M. A., Strain, N. A., and Lee, C. C., "Flight Evaluation of a Stagnation Detection Hot-Film Sensor," AIAA Paper 92-4085, Aug. 1992.

[20]Somers, D. M., Stack, J. P., and Harvey, W. D., "Influence of Surface Static-Pressure Orifices on Boundary-Layer Transition," NASA TM 84492, 1982.

[21]Cox, J., "Cirrus VK30," *Sport Aviation*, Experimental Aircraft Association, Oshkosh, WI, USA, May 1988, pp. 13–18.

[22]Monner, H. P., "Realization of an Optimized Wing Camber by Using Formvariable Flap Structures," *Aerospace Science and Technology*, Vol. 5, No. 7, 2001, pp. 445–455.

[23]Hoadley, A. W., and VanderBok, R. S., "Stall Margin Indication," *Journal of Aircraft*, Vol. 25, No. 4, 1988, pp. 380–383.

[24]Gopalarathnam, A., and McAvoy, C. W., "Effect of Airfoil Characteristics and Trim Considerations on Aircraft Performance," *Journal of Aircraft*, Vol. 39, No. 3, 2002, pp. 427–433.